The Sea Level Response to External Forcings in Historical Simulations of CMIP5 Climate Models*

AIMÉE B. A. SLANGEN, JOHN A. CHURCH, XUEBIN ZHANG, AND DIDIER P. MONSELESAN

CSIRO Oceans and Atmosphere Flagship, Hobart, Tasmania, Australia

(Manuscript received 26 May 2015, in final form 6 August 2015)

ABSTRACT

Changes in Earth's climate are influenced by internal climate variability and external forcings, such as changes in solar radiation, volcanic eruptions, anthropogenic greenhouse gases (GHG), and aerosols. Although the response of surface temperature to external forcings has been studied extensively, this has not been done for sea level. Here, a range of climate model experiments for the twentieth century is used to study the response of global and regional sea level change to external climate forcings. Both the global mean thermosteric sea level and the regional dynamic sea level patterns show clear responses to anthropogenic forcings that are significantly different from internal climate variability and larger than the difference between models driven by the same external forcing. The regional sea level patterns are directly related to changes in surface winds in response to the external forcings. The spread between different realizations of the same model experiment is consistent with internal climate variability derived from preindustrial control simulations. The spread between the different models is larger than the internal variability, mainly in regions with large sea level responses. Although the sea level responses to GHG and anthropogenic aerosol forcing oppose each other in the global mean, there are differences on a regional scale, offering opportunities for distinguishing between these two forcings in observed sea level change.

1. Introduction

More than 90% of the energy accumulated in the climate system over recent decades has been stored in the ocean (Rhein et al. 2013), causing ocean thermal expansion and, together with the addition of mass to the ocean, the rise of sea level. In the past century, global mean sea level has risen by 19 ± 2 cm (1901–2010) and it is projected to rise by another 28–98 cm by 2100 (relative to 1986–2005), depending on the level of anthropogenic greenhouse gas emissions, and potentially several decimeters more if there is a collapse of a portion of the Antarctic Ice Sheet (Church et al. 2013). However, past and future sea level change is not spatially uniform and is projected to locally deviate more than 10% from the global mean in almost 30% of the ocean area (Slangen et al. 2014a).

Studies by Pardaens et al. (2011), Yin et al. (2010), and Yin (2012) have shown that the intermodel spread in twenty-first-century regional sea level projections has been reduced from the previous generation of climate models [phase 3 of the Coupled Model Intercomparison Project (CMIP3; Meehl et al. 2007)] to the current generation [phase 5 of the Coupled Model Intercomparison Project (CMIP5; Taylor et al. 2012)]. They also found a number of robust features in the sea level projections of both model ensembles, such as dynamic sea level rise in high-latitude and polar regions and a beltlike structure in the Southern Ocean. Recent studies by Bouttes et al. (2012, 2014) and Bouttes and Gregory (2014) used a single climate model (FAMOUS) driven by surface fluxes from a range of CMIP3 and CMIP5 models to study regional patterns in sea level under a 1% per year increase in CO_2 concentration scenario to determine the main drivers of change. Recently, Bilbao et al. (2015) identified a scenario-independent sea level

Denotes Open Access content.

* Supplemental information related to this paper is available at the Journals Online website: http://dx.doi.org/10.1175/JCLI-D-15-0376.s1.

Corresponding author address: Aimée B. A. Slangen, CSIRO Oceans and Atmosphere Flagship, GPO Box 1538, Hobart TAS 7001, Australia.
E-mail: aimee.slangen@gmail.com

DOI: 10.1175/JCLI-D-15-0376.1

pattern in response to increasing anthropogenic forcings in sea level projections for the twenty-first century, valid for all representative concentration pathway (RCP) scenarios (Moss et al. 2010). These forced patterns are partly masked by the internal climate variability, which has a larger influence at regional scales than on the global scale (Hu and Deser 2013; Monselesan et al. 2015). Nevertheless, Lyu et al. (2014) found that the anthropogenic signal in total sea level change will emerge from the internal variability by 2020 in 50% of the ocean area.

Earth's climate system is influenced by a range of external forcings, such as anthropogenic greenhouse gases (GHG), ozone, volcanic and anthropogenic aerosols, and changes in solar radiation. Each of these forcings can result in a different response of the climate system and thus potentially lead to a different contribution to the regional pattern of sea level change. The current generation of climate models produce significant, but poorly understood, differences in the regional distribution of sea level change. Determining how each of the individual forcings influences global mean and regional sea level change may assist in identifying the reasons for these differing model responses, leading to improved understanding of the observed regional sea level changes and more robust projections of future regional change. Formal attribution is an important evaluation of the consistency of models with the real world and contributes to increased confidence in projections. Attribution of sea level change also has direct implications for decisions on the mitigation of greenhouse gas emissions.

Using a range of CMIP5 experiments, Slangen et al. (2014b) performed a formal detection and attribution analysis on global mean thermosteric sea level (GMTSL), which is the sea level change caused by density variations as a result of ocean temperature changes. They showed the partition of the observed GMTSL for 1957–2005 between external forcings from natural origin (volcanic eruptions and solar cycles) and from anthropogenic origin (greenhouse gases, ozone, and anthropogenic aerosols). Both this study and a study by Marcos and Amores (2014) unequivocally demonstrated that the majority of the observed GMTSL in the second half of the twentieth century is of anthropogenic origin.

This study extends the analysis presented by Slangen et al. (2014b) to the period 1861–2005 by considering not just the GMTSL, but also the regional sea level patterns. The regional patterns are referred to as the dynamic sea level (DSL) or the sea surface height relative to the geoid, and represent the sea level change because of atmospheric and oceanic circulation changes and as a result of heat and salt redistribution in the ocean. While a number of studies have focused on the DSL in response to future RCP scenarios [which are dominated by GHG forcing (e.g., Bouttes and Gregory 2014; Bilbao et al. 2015)], to date, there are no studies showing the DSL patterns in response to individual anthropogenic forcings or to other external forcings, which are important for our understanding of the observed historical changes. Here, we use CMIP5 climate model simulations for the historical period driven by GHG, anthropogenic aerosol, ozone, and natural forcings, as well as combinations of these, to estimate the influence of external forcings on historical sea level change. Additionally, preindustrial control simulations are used as a measure of the internal climate variability.

The contributions to sea level change from glaciers, ice sheets, groundwater extraction, dam construction, or glacial isostatic adjustment (GIA) are not included in climate models, and are not included in this analysis. However, these contributions are important to include when studying total sea level change, as each can add mass to the ocean and have a significant regional signature, especially close to the source of the mass change (e.g., Church et al. 2013; Slangen et al. 2012, 2014a). During the twentieth century in regions away from the ice sheets (the so-called far field), the high spatial variation of the DSL dominates the relatively smooth spatial patterns that are caused by mass redistribution and their related gravitational, rotational, and deformational effects.

The main question addressed here is as follows: can we identify and explain a robust modeled response in both global mean and regional sea level change to a range of external forcings in historical climate model runs? To answer this question, a large climate model ensemble with five different forcing experiments is used (section 2). Individual model runs are compared to study the impact of internal variability, study the agreement between different climate models, and examine the multimodel ensemble means to identify a robust response to the different external forcings. This will be done for the global mean thermosteric sea level change (section 3) and the dynamic sea level patterns (section 4) over the period 1861–2005.

2. Data and methods

We use output from the CMIP5 climate model database (Taylor et al. 2012; Table 1) and focus on the historical experiments driven by a range of external forcings. The model selection is based on the availability of the dynamical sea surface height variable in at least one external-forcing experiment in addition to the historical experiment (Table 1). There has been no further

TABLE 1. Climate models from the CMIP5 database (Taylor et al. 2012) used in this study, listing the number of model realizations for each forcing experiment.

Model	All forcings	Anthropogenic	Natural	GHG	Anthropogenic aerosol
ACCESS1.3[a]	1	—	—	2	—
CanESM2	5	—	5	5	5
CNRM-CM5[b]	10	10	6	6	—
CSIRO Mk3.6.0	10	10	10	10	10
GFDL CM3	5	3	3	—	3
GFDL-ESM2M	1	1	1	1	1
GISS-E2-R[a,b]	5	5	2	4	5
HadGEM2-ES[a,b]	4	—	4	3	—
IPSL-CM5A-LR[b]	2	3	3	5	1
IPSL-CM5A-MR[b]	2	—	3	3	—
MIROC-ESM[b]	3	—	3	3	—
MIROC-ESM-CHEM[b]	1	—	1	1	—
MRI-CGCM3	3	—	1	1	—
NorESM1-M[b]	3	—	1	1	—
Total no. realizations	55	32	43	45	25
Total no. models	14	6	13	13	6

[a] Wind stress data not available/accessible.
[b] Volcanic forcing included in preindustrial control run.

selection based on model quality, as the reproduction of the observed dynamic sea level climatology by the models gives no clear basis to select a subset of models (Flato et al. 2013, their Fig. 9.16). Although some modeling groups contributed multiple models to the CMIP5 database, possibly causing results not to be fully independent (Knutti et al. 2013), we find that a model selection based on model heritage would not have changed our results (not shown); therefore, all available models are included in our analysis.

Five different forcing experiments are used: 1) natural only (solar and volcanic forcing), 2) anthropogenic only (anthropogenic aerosol, greenhouse gas, and ozone forcing), 3) greenhouse gas only, 4) anthropogenic aerosol only, and 5) historical (including all anthropogenic and natural forcing). In each experiment, one or more forcings are changing with time (e.g., greenhouse gas in the GHG-only experiment), while all other forcings are held constant at their preindustrial levels. There are at least 6 models available for each experiment.

To estimate the internal climate variability, we use the preindustrial control runs (herein called the control runs) of each of the climate models, which are forced by nonevolving preindustrial conditions (Taylor et al. 2009). The available control runs vary in length, ranging from 250 (ACCESS1.3) to 1000 model years (IPSL-CM5A-LR). By using the control runs as an estimate for internal variability, it is assumed that the internal variability is well represented in the climate models. Currently, coupled climate models do not yet have a perfect representation of various modes of climate variability, such as the El Niño–Southern Oscillation (ENSO) or the Pacific decadal oscillation (PDO). However, the simulation of the western tropical Pacific climate variability and processes has improved for the new generation of climate models (CMIP5) with respect to the CMIP3 generation (e.g., Bellenger et al. 2014; Grose et al. 2014). In addition, Monselesan et al. (2015) showed that, for sea level and sea surface temperature, the spatiotemporal characteristics of the variances over various frequencies or bands in the CMIP5 control runs and the observations are in reasonable agreement for those periods and regions where there are reliable observations.

The model variables used here are the GMTSL (CMIP5 variable zostoga), the sea surface height above geoid (CMIP5 variable zos), and the zonal and meridional wind stress from the atmosphere on the ocean (CMIP5 variables tauuo and tauvo). For all monthly model data, we first removed the seasonal cycle by computing the monthly climatology over the full historical period and subtracting that from the time series. Then we computed yearly mean values and dedrifted the data to correct for spurious trends as a result of the model spinup being too short for the ocean to be in equilibrium at the beginning of the experiments (Sen Gupta et al. 2013). To dedrift, a quadratic fit was performed over the full length of the control run, and only the corresponding portion of the fitted drift was removed from the historical experiment at each grid point, taking into account the time correspondence. For zos, the global mean was subtracted at each time step to obtain the DSL, as not all models provide zos with respect to the global mean. Finally, all fields were regridded onto a common $1^\circ \times 1^\circ$ grid using bilinear

interpolation, with a multimodel ensemble land–ocean mask. The longest common time period among all available models for the historical period is 1861–2005.

To create a model ensemble, some climate modeling groups ran the same experiment multiple times with different initial conditions by branching from different points in the control run. This results in multiple realizations, which are also used (in addition to the control simulations) to estimate the internal variability (section 4c). Multimodel ensemble mean values are computed, after the data are processed following the procedures described above, by averaging over all realizations of each model before averaging over the model means such that each model is equally weighted in the multimodel ensemble irrespective of the number of realizations. Although models with few realizations may retain more internal variability than models with a larger number of realizations, the influence on the final multimodel ensemble mean is small, as all models are averaged in the multimodel ensemble anyway.

In section 3, the modeled GMTSL is compared to an observational estimate over the full depth of the ocean for 1957–2005. The observational estimate used is a combination of Domingues et al. (2008, v.3.1; 0–700 m), Levitus et al. (2012, downloaded 7 February 2014; 700–2000 m), and Purkey and Johnson (2010; below 2000 m; 0.1 mm yr^{-1}). Although there are other estimates available for the upper 700 m, such as Levitus et al. (2012) and Ishii and Kimoto (2009), these estimates fall well within the uncertainty range presented by Domingues et al. (2008) and would not lead to different results (Slangen et al. 2014b).

3. Global mean thermosteric sea level change

In the natural-only forced experiment, the GMTSL shows temporary decreases immediately following volcanic eruptions (Fig. 1a). This GMTSL fall is caused by decreased ocean temperatures as a result of negative radiative forcing after volcanic eruptions and is followed by a slow recovery (Church et al. 2005; Gleckler et al. 2006; Gregory et al. 2006). The net GMTSL change in historical simulations with volcanic forcing is dependent on whether or not volcanic forcing was included in the control run, as the omission of volcanic forcing in the control run results in a negative bias in GMTSL when volcanic forcing is introduced in the historical period (Gregory 2010; Gregory et al. 2013). Five models fall into this category [Table 1, from Table 12.3 in Collins et al. (2013)], of which four models show a GMTSL fall of 0–0.03 m over the historical period, in agreement with the AOGCM experiments of Gregory et al. (2013). Only the CSIRO Mk3.6.0 model does not follow this pattern and, for unknown reasons, has a small net GMTSL increase despite having no volcanic forcing in the control run. For the simulations that do include an average volcanic forcing in the control run, the net change over 1861–2005 is less than 0.01 m in the natural-only experiment.

Compared to observations, the GHG-only forced experiment (Fig. 1b) results in an overestimated GMTSL rise of 0.09 ± 0.02 m, while the negative radiative forcing effect of anthropogenic aerosols and the resultant decrease in ocean heat content is associated with a substantial GMTSL fall of 0.05 ± 0.03 m (Fig. 1c). The rate of GMTSL change for the GHG experiment increases sharply from 1950 onward and reaches nearly 2 mm yr^{-1} in 2005. The shape of GMTSL in the GHG experiment closely follows the evolution of atmospheric GHG radiative forcing (Myhre et al. 2013, their Fig. 8.6). The aerosol experiments show an acceleration in the negative rate of GMTSL change after 1950 down to around -1 mm yr^{-1} in 2000. The changes in GMTSL rate agree with the temporal evolution of the aerosol radiative forcing (Myhre et al. 2013, their Fig. 8.8), which increases slowly until 1950, then accelerates and stabilizes after 1990. Note also the larger model spread in aerosol-only simulations compared to GHG-only simulations, because of the larger uncertainty in the aerosol–radiative forcing response in the climate models (Myhre et al. 2013).

The anthropogenic experiment includes GHG, anthropogenic aerosol, and ozone forcing. The aerosol forcing mitigates most of the GHG forcing until 1960, but after 1960 the GHG forcing becomes larger and the rates of change increase to 1 mm yr^{-1} in 2005. As a result of the combined forcing, the anthropogenic-only GMTSL (Fig. 1d) is in much closer agreement with the observed GMTSL than the natural, GHG, or aerosol-only GMTSL. The anthropogenic simulations lack the response to volcanic eruptions as natural forcings are excluded, resulting in a smoother GMTSL change than observed.

The historical experiment (Fig. 1e) agrees well with the observed changes over the period 1957–2005. This agreement confirms the results of Slangen et al. (2014b), while here the modeled GMTSL is shown for fewer models but over a much longer period. The temporal variability in GMTSL across all models is consistent with the response to volcanic forcing.

By combining the information of the forcing experiments, differences in the historical simulations can be better understood. For example, for GFDL-CM3 (Fig. 1, solid magenta line) we have no GHG experiment available, but, using the other experiments, it can be deduced that the GMTSL response to GHG forcing must be of opposite sign and slightly larger magnitude

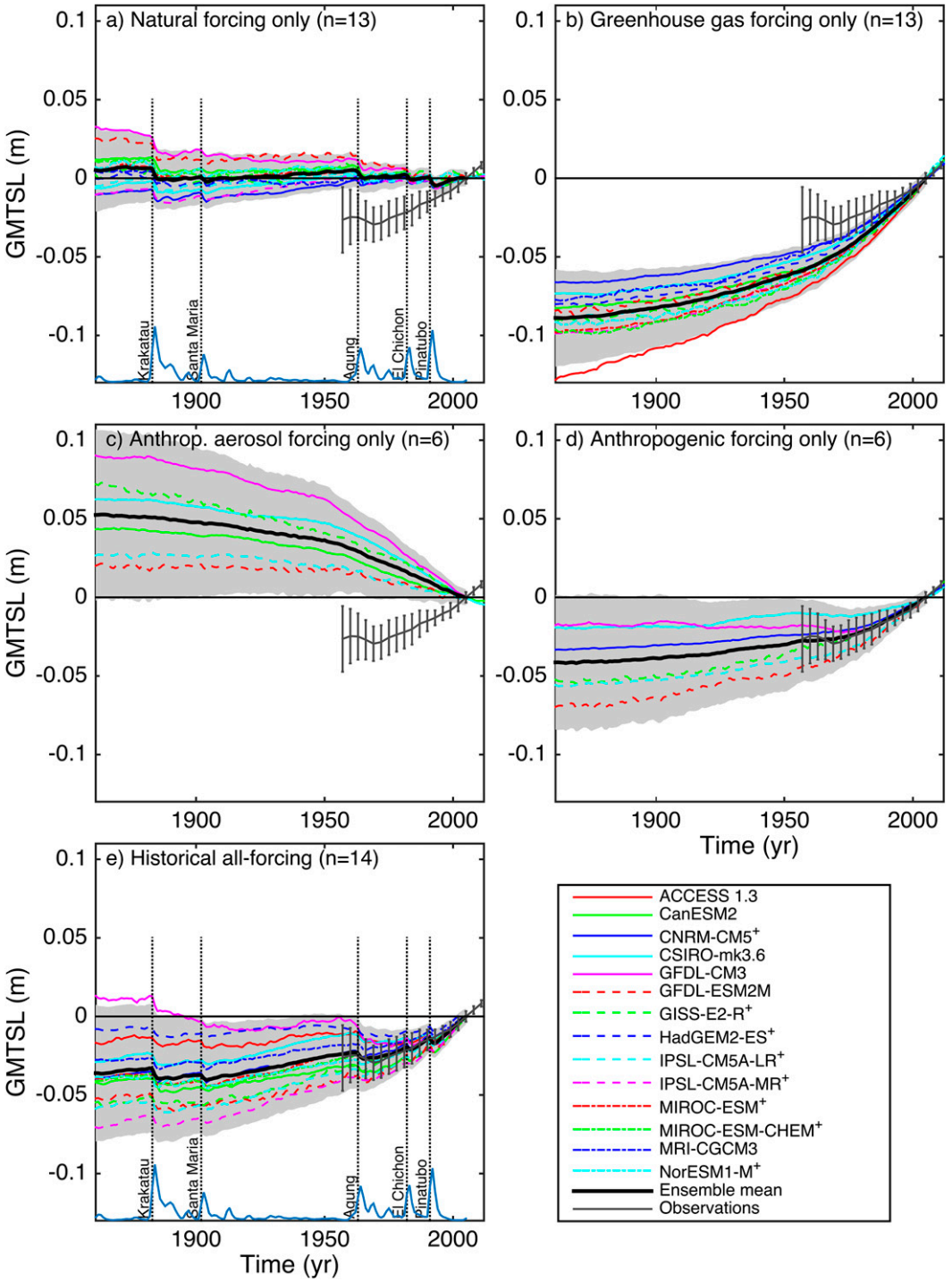

FIG. 1. Full-depth GMTSL (m) 1861–2005 (individual models extended to 2012 where possible). Multimodel mean (black), $\pm 2\sigma$ model spread (gray shading, including control run uncertainty), model means (color), and observations (dark gray) [Domingues et al. (2008), 0–700 m; Levitus et al. (2012), 700–2000 m; and Purkey and Johnson (2010), >2000 m]. (a) Natural only, indicating volcanic radiative forcing (blue; arbitrary scale; multiplied by −1) and major volcanic eruptions (vertical dashed lines) (Meinshausen et al. 2011), (b) GHG only, (c) anthropogenic aerosol only, (d) anthropogenic only, and (e) historical. Models marked $^+$ include volcanic forcing in the preindustrial control run.

than the GMTSL aerosol response. For the ACCESS1.3 model (Fig. 1, solid red line) there is no aerosol-only experiment, but the information of the GHG and anthropogenic experiments implies that the GMTSL response to aerosol forcing in this model must be large (Lewis and Karoly 2014).

4. Regional patterns in dynamic sea level change

a. Ensemble mean trend patterns

While the internal climate variability has a relatively small effect on GMTSL, it can be larger regionally (Hu and Deser 2013), mainly on shorter (up to multidecadal) time scales, but also on centennial time scales (Carson et al. 2015; Bordbar et al. 2015; Monselesan et al. 2015). We have compared DSL trends for the five different forcing experiments over various periods and find that, while the overall response to the external forcings is consistent, the patterns show more variability over shorter (decadal to multidecadal) periods because of the larger influence of internal climate variability. On centennial time scales, the effect of internal variability is much smaller, allowing for a better quantification of the response to external forcings; therefore, the DSL patterns are studied over the longest time period available in the historical simulations (1861–2005).

To fully sample the range of internal variability in DSL trends in the control runs, 50 trends of 145 yr (same length as the 1861–2005 period) are randomly drawn from each of the 14 control runs, which is about once every 2 yr in the shortest control run, up to once every 15 yr in the longest control run. The multimodel ensemble mean DSL trend in the control runs is near zero (Fig. 2a, left), showing that the internal variability on centennial time scales averages out in the ensemble mean. There is some spread in the DSL trends (Fig. 2a, middle), mainly in the high latitudes, caused by a combination of model differences and internal variability. This agrees with Monselesan et al. (2015), who found that the variance in the DSL control runs moves from middle to higher latitudes on progressively longer time scales. As the ensemble mean internal variability DSL trend is near zero and smaller than the standard deviation of the trend, the signal-to-noise ratio is also small (Fig. 2a, right).

In the natural-only experiments, the ensemble mean DSL trend is small (Fig. 2b) but slightly larger than the control run trends (Fig. 2a). The main difference compared to the control runs is the addition of forcing from episodic volcanic eruptions and the 11-yr solar cycle. The spread of the natural-only forced DSL trends is similar to the control run spread, while the signal-to-noise ratio is below 1 everywhere, as the ensemble spread is larger than the ensemble mean. If the natural-only experiment standard deviation is replaced by the standard deviation of the control runs, all values are smaller than 1, indicating that the natural-forced ensemble mean DSL trend is also within the range of internal climate variability.

In contrast to the natural-only and control experiments, each of the experiments that includes anthropogenic forcing does show long-term DSL trends in the ensemble mean. The GHG ensemble mean DSL trend (Fig. 2c) closely resembles the Bouttes et al. (2014) projected twenty-first-century DSL under a 1% yr^{-1} increase in CO_2 scenario, both showing a Southern Ocean dipole (e.g., Yin et al. 2010), a North Atlantic dipole (e.g., Yin et al. 2009), and an increase in the low-latitude western Pacific. A similar pattern is also found in Bilbao et al. (2015) using RCP scenarios for the twenty-first century, which mainly include GHG forcing, indicating that the GHG-forced DSL pattern is robust in time. The anthropogenic aerosol-forced DSL trend (Fig. 2d) is almost a mirror image of the GHG-forced trend, though not exactly. Most of the Southern Ocean shows a sea level rise where the GHG forcing causes a sea level fall, although the Southern Ocean dipole is not perfectly mirrored, and aerosol-only forced DSL trends are smaller. In the Indian Ocean and the North Pacific, the negative DSL trend in the aerosol experiments opposes the positive GHG-forced response. The anthropogenic ensemble mean trend (Fig. 2e), which is driven by both anthropogenic aerosol and GHG forcing, resembles a reduced-amplitude version of the GHG-forced trend pattern, especially in the Southern Ocean. The historical DSL ensemble mean trend (Fig. 2f) is similar to the anthropogenic-forced DSL trend, indicating that most of the DSL change in the historical experiment is driven by anthropogenic forcing, as was the case for the GMTSL.

For each of the anthropogenically forced experiments, the ensemble spread in DSL trend is larger than in the control and natural-only experiments (Fig. 2, middle). This shows that the ensemble spread is not a measure of internal variability alone, but also of the different model responses to external forcing. The standard deviation in the DSL trends is largest in the high latitudes, where the ensemble mean trend is large, while it is smaller (0–0.2 mm yr^{-1}) in the 30°N–30°S region. For the four experiments that include anthropogenic forcing (Figs. 2c–f), the signal-to-noise ratio is larger than 1 in parts of the North Pacific and most of the Southern Ocean, although the exact location differs between the experiments. Areas with a signal-to-noise ratio larger than 2 are sparser. The ratio doubles when

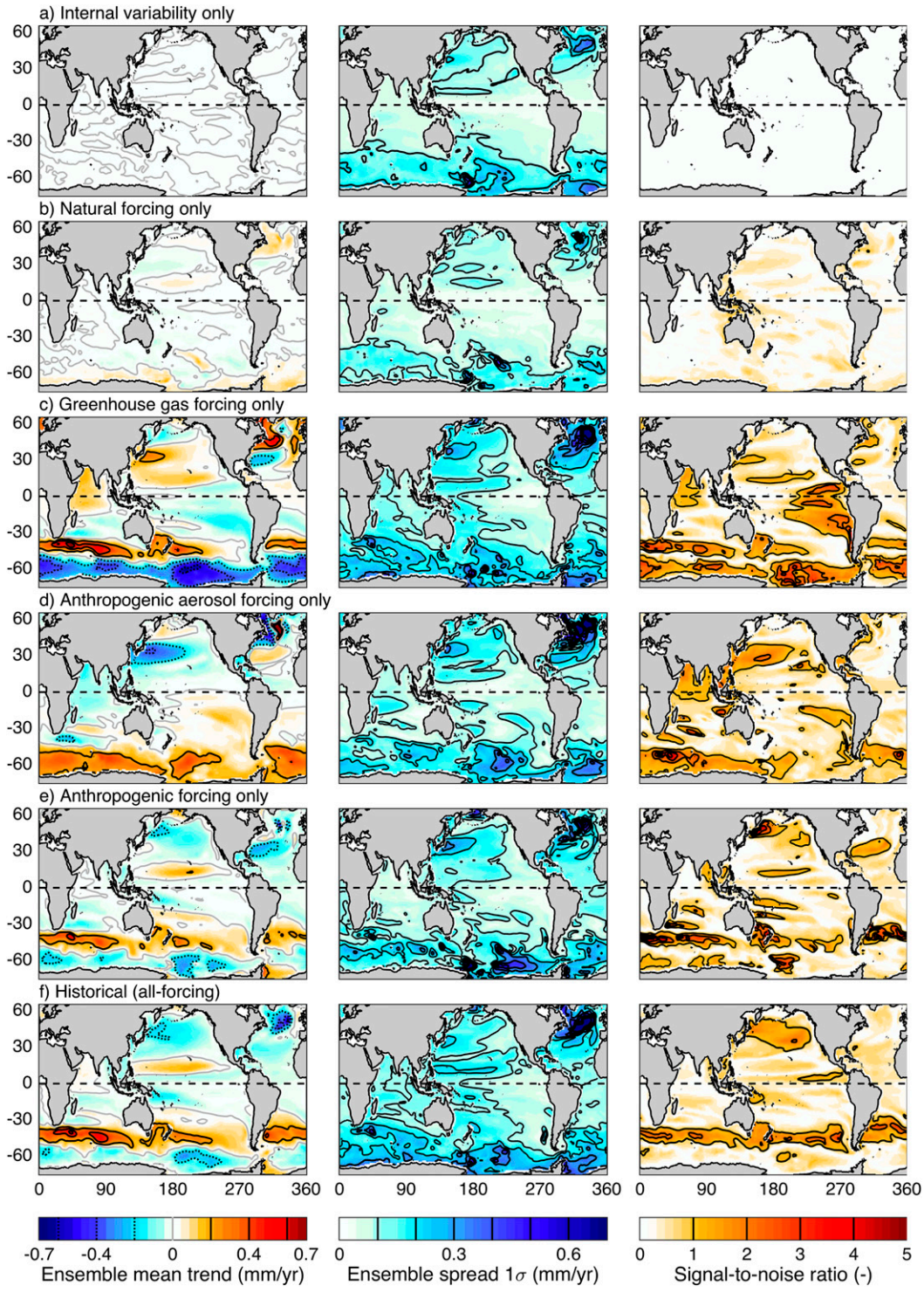

FIG. 2. Multimodel ensemble mean (left) linear DSL trends (mm yr^{-1}), (middle) spread of multimodel ensemble trends (1σ; mm yr^{-1}), and (right) the signal-to-noise ratio (mean σ^{-1}) for 1861–2005. (a) Internal variability only, (b) natural only, (c) GHG only, (d) anthropogenic aerosol only, (e) anthropogenic only, and (f) historical.

the noise is replaced by the standard deviation of the DSL trend in the control run, indicating that the variation in the experiment patterns is significantly larger than internal variability. The signal-to-noise ratio is not significantly different for DSL trends over shorter periods.

b. *Ensemble mean EOF analysis*

In addition to the ensemble mean DSL trends, the modes of variability are computed with empirical orthogonal function (EOF) analysis (Fig. 3), which has the advantage that the principal component (PC) time series indicate how the strength of the spatial field varies with time. The EOFs are computed for the multimodel ensemble means of each of the five historical experiments, for yearly and pentadal DSL time series. The multimodel ensemble mean of the first 145 yr of the dedrifted control runs is used to compute the EOFs of the internal variability.

The leading EOFs of the yearly time series of the control runs (Fig. 3a) and of the natural-only experiment (Fig. 3b) show an ENSO-like pattern in the Pacific and a weak dipole in the Atlantic, consistent with changes in the Atlantic meridional overturning circulation (AMOC). In contrast, the leading EOF of the pentadal time series of the natural-only experiment (not shown) has a slightly stronger signal in the midlatitudes, consistent with a PDO/interdecadal Pacific Oscillation signal (Mantua et al. 1997; Power et al. 1999). The leading EOF is stronger in the natural experiment than in the control runs, possibly because of the presence of synchronized external forcing (solar cycle and volcanic eruptions).

In the literature, there is an ongoing discussion if and how volcanic eruptions can influence internal climate variability. Robock (2000) showed how volcanoes can cause short-term cooling on a global scale for up to a couple of years from one eruption or up to a century from multiple eruptions, but finds little evidence that volcanic eruptions can trigger El Niños. On decadal time scales, Stenchikov et al. (2009) found that volcanic forcing strengthens the AMOC in the GFDL CM2.1. More recently, Swingedouw et al. (2015) showed that volcanic forcing in CMIP5 simulations over the latter half of the twentieth century can reset multidecadal variability in the North Atlantic such that volcanic forcing is responsible for the timing of the Great Salinity Anomalies in the 1970s and 1990s. There is also paleo evidence of excitation of bidecadal North Atlantic variability following earlier eruptions. In contrast to Robock (2000), Mann et al. (2005) argue for an increased likelihood of El Niño events the year after volcanic eruptions in a large model ensemble (100 realizations), particularly for more powerful eruptions. However, they find that this effect is relatively weak in the twentieth century.

The PC time series of the natural-forced experiment DSL (Fig. 3b) shows an increase (more El Niño-like conditions) the year following larger volcanic eruptions, in agreement with Mann et al. (2005). On a decadal time scale, all eruptions (except El Chichon in 1982) result in a decrease in the PC consistent with a strengthening of the AMOC, in line with Stenchikov et al. (2009) and Swingedouw et al. (2015). However, there is also considerable internal variability in the PC time series that is not linked to volcanic eruptions.

For each of the experiments that include anthropogenic forcing, the leading EOF patterns (Figs. 3c–f, left column) are similar to their ensemble mean DSL trends (Figs. 2c–f, left column). There is no linear trend present in the higher-order PCs, indicating that most of the forced response is in the first EOF. We find that both methods agree on the forced response of the DSL trend. Again, the Southern Ocean dipole in response to GHG forcing dominates the anthropogenic and historical DSL pattern and is only partly mitigated by the anthropogenic aerosol forcing. The same leading EOF patterns and PC time series are found for yearly and pentadal data (Figs. 3c–f, right column), and the PCs show increasing strength (in time) of the leading EOF modes. The explained variance of the pentadal time series is larger (+18%–26%), because the pentadal averaging filters out some of the short-term variability, which in the yearly time series will be placed in a higher EOF mode. The explained variance of the GHG experiments is the largest, possibly as a result of the strong GHG forcing and less spatial and temporal variability in the model response.

We compute the correlation coefficients of the leading EOF patterns of the five experiments with the historical ensemble mean DSL time series to determine which forcings drive the historical DSL changes [Fig. 4, analogous to Fig. 8 in Bilbao et al. (2015)]. The 5%–95% internal variability interval (gray shading) is constructed from correlations of the control runs with each of the five leading EOFs. The natural-only correlation coefficients (green) do not emerge permanently from the internal variability but do show increases after volcanic eruptions, as the historical DSL pattern is temporally more influenced by natural forcing. The correlations of all anthropogenically forced experiments temporally decrease (the aerosol correlation time series becoming less negative) after volcanic eruptions. The aerosol-only correlation coefficients (cyan) do emerge from the internal variability at times but nevertheless appear to be difficult to identify in the historical DSL patterns,

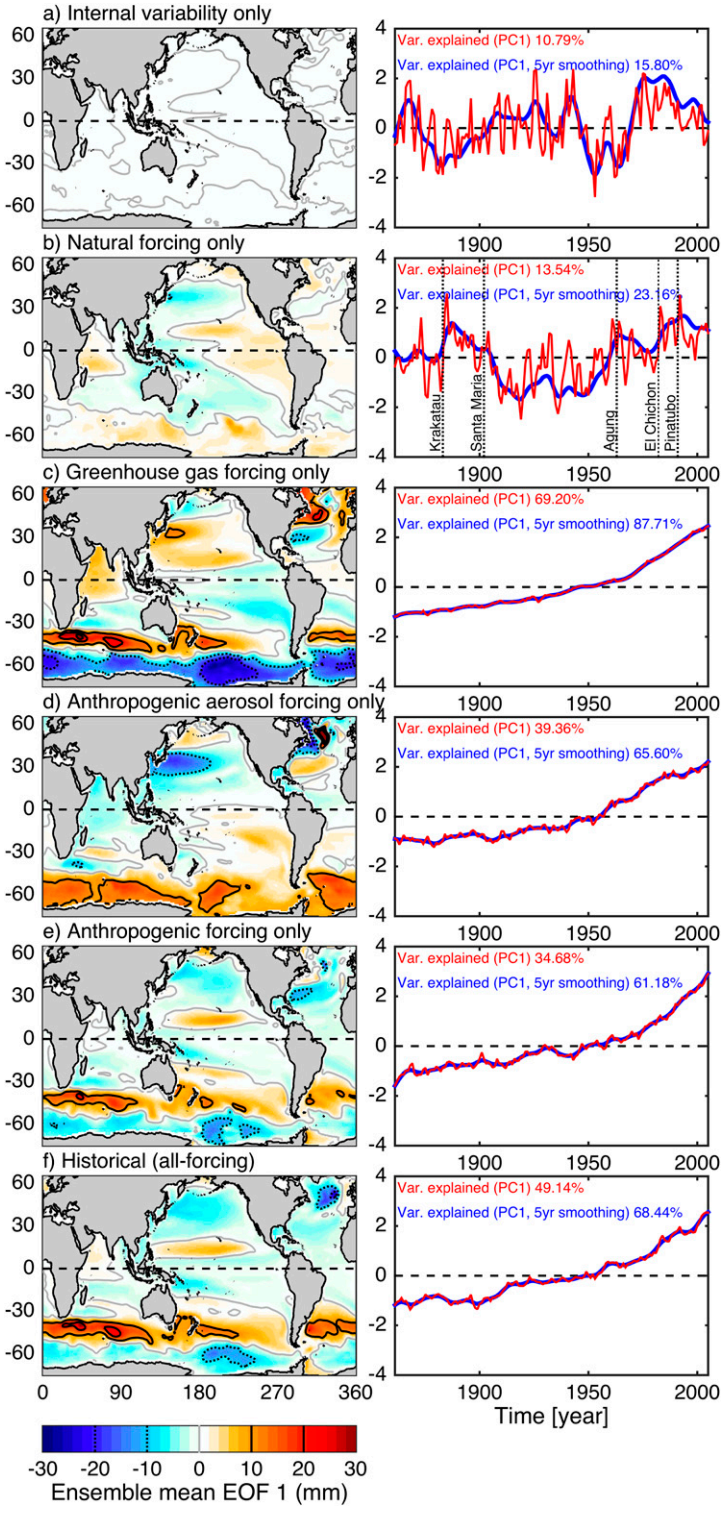

FIG. 3. (left) Leading EOF of yearly multimodel ensemble mean DSL (mm), and (right) the associated PC time series for yearly (red) and 5-yr running mean (blue) EOF analysis (1861–2005). (a) Internal variability only, (b) natural only (including major volcanic eruptions), (c) GHG only, (d) anthropogenic aerosol only, (e) anthropogenic only, and (f) historical.

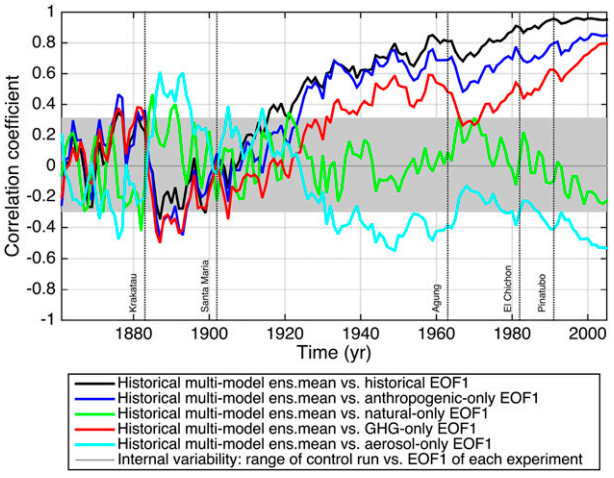

FIG. 4. The correlation coefficients of the historical DSL ensemble mean with the leading EOF patterns of the five forcing experiments as presented in Fig. 3. The shaded band indicates the internal variability (5th–95th percentile), obtained by correlating the preindustrial control runs to the leading EOFs; black dashed lines represent the major volcanic eruptions.

probably because part of the aerosol response is obscured by the stronger and partially opposing GHG response. The GHG-only correlation (red) reaches 0.8 and the anthropogenic-only correlation (blue) is even larger, as this EOF includes most of the relevant forcings. The highest correlations are with the leading EOF of the historical time series itself (black), reaching almost 1 by 2005. Before 1930, the correlations of the historical DSL time series with all three EOFs that include GHG forcing are highly variable and even partly negative, although mostly within the range of internal variability. The actual GHG forcing and the resulting DSL response is still small in this period, and it is likely that the DSL is still mostly influenced by internal variability. Later in the twentieth century, the GHG forcing increases as well as the DSL (and GMTSL, Fig. 1) response, leading to higher correlation coefficients between the leading EOFs and the historical time series.

c. *Internal variability in the models*

Out of the 52 model–experiment combinations (Table 1), there are 34 with at least three realizations available for the same experiment. From this subset, the first realization of each model–experiment combination (supplementary Figs. S1–S5) is compared to the corresponding model mean and model standard deviation; Fig. 5 shows one randomly selected model for each experiment. A comparison of the standard deviation within the models (Fig. 5, middle) to the standard deviation of the control runs (Fig. 5, right, constructed by computing the DSL trend over fifty 145-yr sections from the control run to obtain a representative sample of the internal variability) shows that, irrespective of the model or experiment choice, the spread between realizations is similar to the internal variability, both in terms of spatial patterns and magnitude. This indicates that within each model the individual realizations respond similarly to the same external forcing. This is true for all model–experiment combinations in this study with at least three realizations. In addition, the similarity between realization spread and control run spread indicates that the external forcings do not influence the internal variability (about a possibly changing mean field) substantially, suggesting there are no or little feedbacks between the forcings and internal climate modes in the models in the historical period for DSL. However, model projections suggest that there may be some changes in climate phenomena such as ENSO in the future (Christensen et al. 2013), and Lu et al. (2014) suggest that for surface air temperature there is a two-way interaction between forced and internal climate variability in climate models. The spread in the multimodel ensembles (Fig. 2, middle) is larger than the spread within the individual models (Fig. 5, middle), which means that the different response of each of the models is responsible for uncertainties in addition to the internal variability.

d. *Linearity in the response to external forcing*

Detection and attribution studies [see, e.g., Bindoff et al. (2013), and references therein] implicitly assume that different forcings can be either applied separately or combined and that feedback effects are negligible. To see how much of the signal is explained by linear additions of the response to external forcing, we compare the sum of the natural and anthropogenic experiments to the historical experiment (the historical comparison) and the sum of the GHG and aerosol experiments to the anthropogenic experiment (the anthropogenic comparison). We select the models that provide all three experiments needed: six models in the historical comparison and four models in the anthropogenic comparison.

First, root-mean-square differences (RMSD, weighted for ocean area) are computed for both cases to compare the summed DSL trends (e.g., natural + anthropogenic) to the full DSL trends (e.g., historical). This is done for the multimodel mean, for model means, and for individual realizations (Table 2). The RMSDs of the individual model realizations and the model means are on the order of 0.10–0.20 mm yr^{-1}, which is 5%–20% of the total range of DSL trends. The multimodel ensemble mean RMSDs are smaller as they are less influenced by internal climate variability: 0.07 and 0.14 mm yr^{-1} for the historical and anthropogenic comparison, respectively.

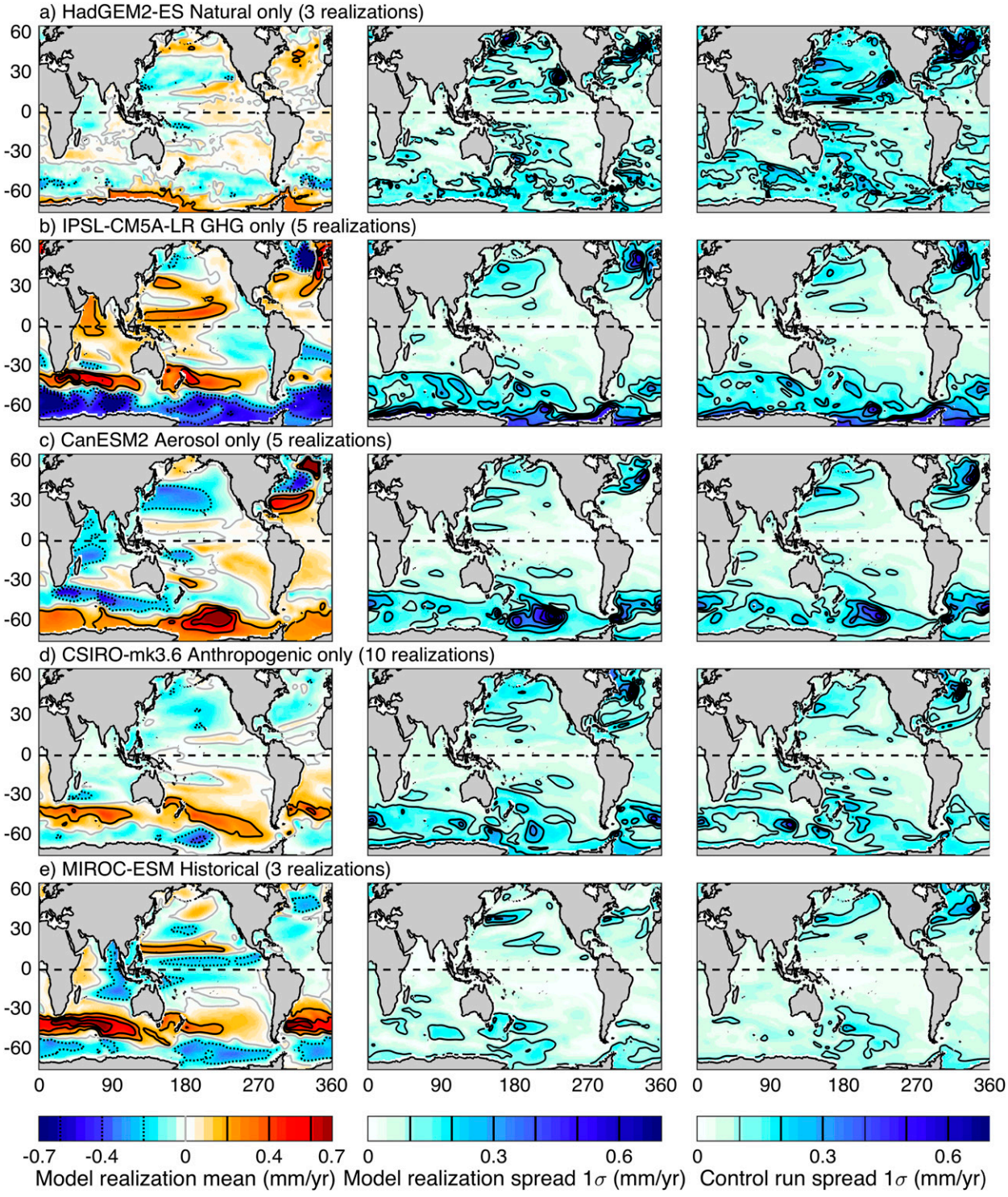

FIG. 5. Model realizations (left) mean linear DSL trends (mm yr^{-1}), (middle) spread of multirealization trends (1σ; mm yr^{-1}) and (right) spread in 50 control run trends (1σ; mm yr^{-1}) for 1861–2005 for five randomly selected models. (a) Natural only (HadGEM2-ES), (b) GHG only (IPSL-CM5A-LR), (c) anthropogenic aerosol only (CanESM2), (d) anthropogenic only (CSIRO Mk3.6.0), and (e) historical (MIROC-ESM).

TABLE 2. Root-mean-squared difference (mm yr^{-1}) for the sum of the natural and anthropogenic experiment vs the historical experiment and the sum of the GHG and aerosol experiment vs the anthropogenic experiment for model means and individual realizations.

Historical vs natural + anthropogenic		
Model	Model mean	Individual realizations
CNRM-CM5	0.07	0.14, 0.15, 0.17, 0.17, 0.15, 0.13
CSIRO Mk3.6.0	0.04	0.20, 0.13, 0.11, 0.12, 0.16, 0.18, 0.15, 0.14, 0.16, 0.19
GFDL CM3	0.07	0.15, 0.12, 0.16
GFDL-ESM2M	0.15	0.15
GISS-E2-R	0.16	0.20
IPSL-CM5A-LR	0.11	0.22, 0.17
Anthropogenic vs GHG + aerosol		
Model	Model mean	Individual realizations
CSIRO Mk3.6.0	0.09	0.13, 0.18, 0.14, 0.18, 0.16, 0.18, 0.18, 0.16, 0.15, 0.19
GFDL-ESM2M	0.22	0.22
GISS-E2-R	0.14	0.19, 0.22, 0.20, 0.22
IPSL-CM5A-LR	0.13	0.29

The RMSDs of the historical comparison are generally smaller than those of the anthropogenic comparison.

For the multimodel mean DSL trend pattern, based on 1 realization per model, we find that the majority of the signal is explained by linear addition of the forced responses. Only 6% of the grid points in the historical comparison (Fig. 6c) have a difference of more than 1σ of the multimodel ensemble spread and 29% in the anthropogenic comparison (Fig. 6e). In the historical comparison (Figs. 6a–c), the differences are relatively small and occur in regions with larger DSL signals, such as the Southern Ocean and the North Atlantic. The individual model simulations (not shown) are less smooth, but the largest differences occur in the same regions, although the magnitude and the sign may vary. The anthropogenic comparison (Figs. 6d–f) shows larger and

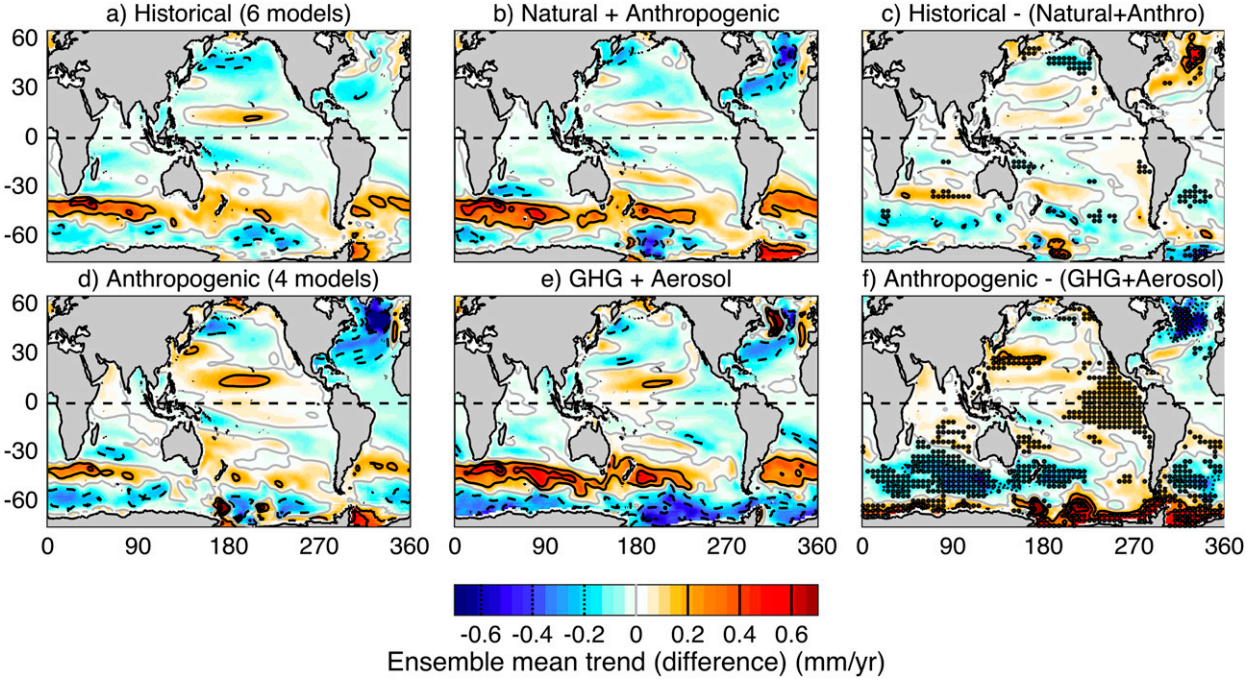

FIG. 6. Ensemble mean linear DSL trends (mm yr^{-1}; 1861–2005): (a) Historical compared to (b) anthropogenic + natural, and (c) the difference between (a) and (b) (first realization of six models in Table 2). (d) Anthropogenic compared to (e) GHG + anthropogenic aerosol, and (f) the difference between (c) and (d) (first realization of four models in Table 2). (c),(f) Stippled for abs(difference) >1σ spread in the multimodel ensemble (containing six and four models, respectively).

more widespread differences (Fig. 6f) than the historical comparison (Fig. 6c). Similar differences are found in the individual model simulations (not shown).

One reason for the larger differences in the anthropogenic comparison is that there are anthropogenic forcings that are not included in the GHG and aerosol (GHG + aerosol) experiments, such as changes in land use or ozone concentrations. Also, in the historical comparison, a large signal (the anthropogenic forcing) is added to a small signal (the natural forcing), so the anthropogenic forcing dominates the response, and the resulting differences caused by additional feedbacks are small (Fig. 6c). In the anthropogenic comparison however, two signals of comparable magnitude are combined (GHG and aerosol forcing), which may cause feedback effects to be larger (Fig. 6f). The short lifetime of aerosols and the complexity of their interaction with other forcing agents may also lead to feedback effects (Myhre et al. 2013). Without dedicated single-forcing experiments of these contributions, it is not possible to say whether the differences in the anthropogenic comparison are caused by unresolved contributions and/or nonlinear feedback effects.

e. *Differences in zonal mean trends*

The climate models in the CMIP5 database have differences in resolution, subgrid parameterizations, implementation of forcing agents in the experiments (aerosol and cloud schemes), and different combinations of ocean and atmosphere models. This section uses the zonal mean DSL trends to simplify the complex spatial DSL patterns, to identify the most robust features for each experiment, and to understand the differences between the models. In this section, the first available realization of each model is used to show the robustness of the trends in individual models, and the ensemble mean is based on these first realizations only. The internal variability is estimated by sampling 50 zonal 145-yr trends from each of the control runs.

While the zonal DSL trends of the natural experiment (Fig. 7a) are entirely within the range of internal variability, the experiments that include anthropogenic forcing (Figs. 7b–e) show values larger than the internal variability in all models. The largest trends are in the Southern Ocean in all models irrespective of which forcing is applied and even with just control run variability, implying that internal variability can induce trends in DSL at centennial time scales in the Southern Ocean (O'Kane et al. 2013). The location of the peaks is more consistent across models in the GHG experiment (Fig. 7b, around 41°S and 69°S) than in the anthropogenic and historical experiments (Fig. 7d,e; see also supplementary Figs. S1 to S5, which show the individual model DSL patterns). This difference is caused by the larger spread in the response to aerosol forcing (Fig. 7c, supplementary Fig. S3), which leads to a positive response south of 41°S. Although the correlation between the GHG and aerosol multimodel means is high and mainly driven by the Southern Hemisphere (−0.76; −0.47 for NH; −0.76 for SH), it also indicates that the DSL response to GHG and aerosol forcing is not a perfect mirror image, offering some hope to separate the aerosol and GHG responses. For instance, the minimum of the GHG is around 69°S, while the maximum of the aerosol experiment occurs around 58°S, which results in a negative peak around 62°S in the anthropogenic experiment and also a change in shape of the zonal mean trend. The positive GHG peak around 41°S, on the other hand, is not mitigated by the aerosol experiment at all, as these are close to zero, resulting in a positive trend in the anthropogenic experiments.

The experiments that include anthropogenic forcing (Figs. 7b–e) also show larger variability north of 20°N, albeit less than in the Southern Ocean. These zonal trends are a trade-off between changes in the North Pacific and the North Atlantic. In the Pacific, the regional patterns show a negative DSL around 30°N and a neutral-to-positive DSL around 50°N under aerosol-only forcing (supplementary Fig. S3). This is reversed in most of the GHG experiments (supplementary Fig. S2). In the combined anthropogenic experiments (supplementary Fig. S4), sometimes the response to GHG forcing is the stronger effect (GFDL-ESM2M, GISS-E2-R, and IPSL-CM5A-LR), and sometimes the response to aerosol forcing is (GFDL CM3 and CSIRO Mk3.6.0). In the North Atlantic, most models show a strong response to the aerosol forcing, with a tendency for a positive–negative–positive tripolar structure. Under GHG forcing, this region is strongly influenced as well, although not exactly opposing the response to the aerosol forcing. Some models show an opposing tripolar structure (e.g., CanESM2 and MIROC-ESM), while others tend toward a dipole (e.g., CSIRO Mk3.6.0 and GFDL-ESM2M) or even a mostly positive or negative North Atlantic DSL trend (CNRM-CM5 and ACCESS1.3).

5. Discussion

a. *Wind stress as a driver of sea level change*

Many studies have been conducted on the underlying mechanism that connects the changes in external forcing to the sea level, using a range of models, and focusing on different regions. For instance, in the Indian and Pacific Oceans it was shown that DSL change is mainly driven by wind stress, using either a simplified dynamical ocean

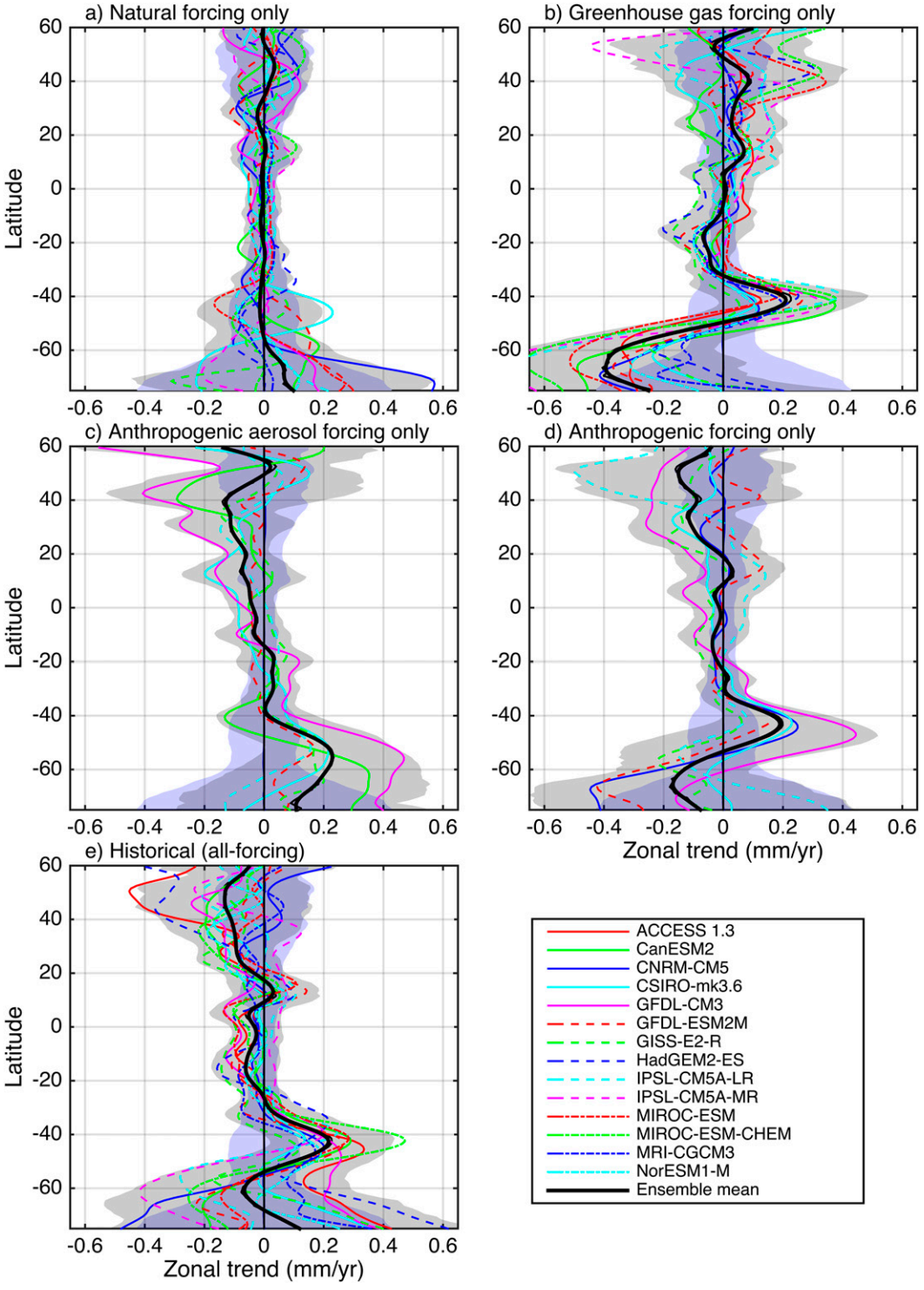

FIG. 7. Zonal average trends (mm yr^{-1}; 1861–2005; 5° smoothed meridionally): (a) natural only, (b) GHG only, (c) anthropogenic aerosol only, (d) anthropogenic only, and (e) historical. Internal variability (2σ; blue shading) based on 50 randomly drawn zonal mean 145-yr trends from each preindustrial control run. Model first realizations (in color) and multimodel ensemble mean and spread (black line and gray shading; $\pm 2\sigma$).

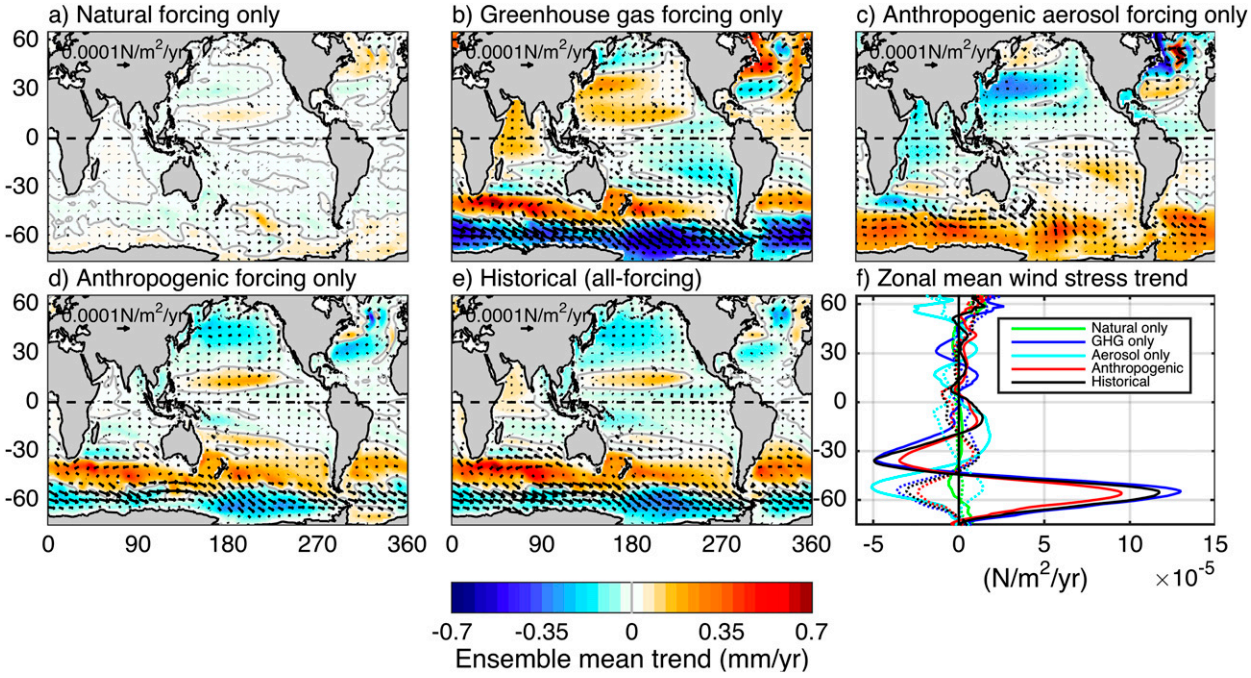

FIG. 8. Multimodel ensemble mean linear DSL trends (shading and contours; mm yr^{-1}) and the wind stress trend from the atmosphere onto the ocean (vectors, N m^{-2} yr^{-1}) for 1861–2005. (a) Natural only, (b) GHG only, (c) anthropogenic aerosol only, (d) anthropogenic only, (e) historical, and (f) zonal mean wind stress trend of all experiments in zonal (solid lines) and meridional direction (dashed lines). Note that DSL and wind stress are both shown for a reduced number of models because of reduced availability of wind stress data (Table 1).

model (Timmermann et al. 2010) or an ocean general circulation model (Nidheesh et al. 2013). In addition, Piecuch and Ponte (2011, 2012) pointed out that buoyancy forcing is important to explain interannual variability in sea level in both the tropical Atlantic and the tropical Pacific regions. Using AOGCMs, Bouttes et al. (2012, 2014) and Bouttes and Gregory (2014) found that changes in sea level can mostly be explained by wind stress (e.g., in the Southern Ocean) but also by heat (e.g., in the North Atlantic) and freshwater fluxes (e.g., in the Arctic Ocean). In the Southern Ocean, Böning et al. (2008) found that observed changes in the Antarctic Circumpolar Current transport can be partly explained by trends in heat and freshwater fluxes but that there is also a strong effect of a wind-induced increase in the eddy fluxes as simulated by eddy-resolving models. More recently, Frankcombe et al. (2013) used an eddy-permitting model and found that sea level falls around Antarctica as a result of increasing westerly winds that are moving poleward, which corresponds to a positive shift in the southern annular mode.

Although the importance of the different drivers seems to vary depending on the type of model and the region studied, it is clear that wind stress changes are one of the main drivers of dynamic sea level change. Indeed, the magnitude and shape of the DSL trend closely corresponds to changes in wind stress in each of the five different experiments for the period 1861–2005 (Fig. 8). For the natural-only experiment, both the wind stress changes and the DSL trends are small. The wind stress trends in the experiments that include GHG forcing agree with the results of Bouttes et al. (2012) and Frankcombe et al. (2013) and show a poleward intensification in the wind stress (Figs. 8b,d,e). The zonal component of the wind stress is larger than the meridional component (Fig. 8f), with the peaks in the Southern Ocean within 1° difference for the GHG, anthropogenic, and historical experiments. The wind stress curl indicates the divergence/convergence zones in the wind stress in the Southern Ocean, and these match the zonal DSL peaks in Fig. 7. The driving effect of the wind stress is strongest in the GHG-only experiment but is also large in the anthropogenic and historical experiments. In the aerosol experiment, the Southern Ocean wind stress trends weaken and show an opposite direction to the GHG-forced wind stress trends, causing a sea level rise around Antarctica instead.

b. *Correlation of GHG and anthropogenic aerosol responses*

Previously, Slangen et al. (2014b) found that GHG and aerosol forcing have opposing effects with a similar

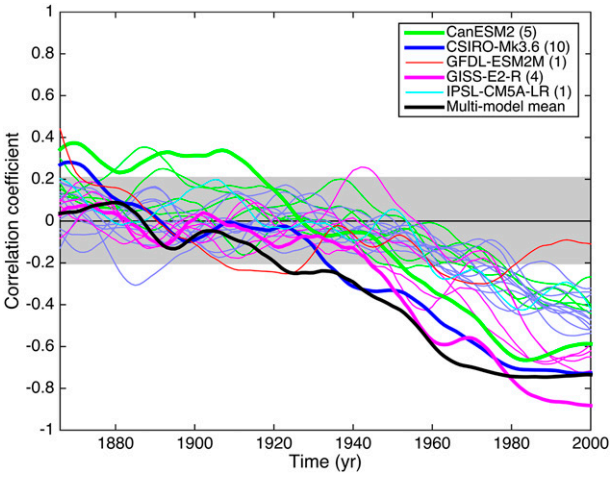

FIG. 9. Correlation coefficients (10-yr smoothed from yearly correlation coefficients for clarity) of GHG vs aerosol DSL time series, for multimodel mean (black), model means (thick colored lines), and individual realizations (thin colored lines) for 1866–2000 (first and last 5 yr discarded to avoid end effects from smoothing). Gray shading reflects the 5th–95th percentile of internal variability, based on correlations of the preindustrial control runs w.r.t. GHG and aerosol multimodel ensemble mean DSL.

time evolution in the GMTSL for the period 1957–2005. Actually, the correlation coefficient of ensemble mean GMTSL is <-0.99 for every time period starting 1861–2004 and ending in 2005 ($p \sim 0$), and GHG $\sim= -1.57 \times$ aerosol for 1861–2005. Individual realizations and model mean GMTSL time series also have correlation coefficients between -0.97 and -0.99. Clearly, with such high correlations it is not possible to separate the contributions from these two forcing agents to GMTSL.

In contrast, the DSL trends from the GHG and aerosol experiments (Figs. 2c,d) do not mirror each other completely, reflected by a correlation coefficient of -0.78 ($p \sim 0$) and a zonal mean trend correlation of -0.76. For the five models with GHG and aerosol-only experiments, the correlation coefficients for the model mean trends are around -0.7, while, for the individual realizations, the values are closer to -0.5, because individual realizations are influenced more by internal variability than the intramodel or multimodel means.

The temporal evolution of the spatial correlation between GHG- and aerosol-forced DSL may provide better opportunities to separate the two forcings (Fig. 9; correlations 10-yr averaged for clarity). For individual simulations (thin lines) before the 1960s, the correlations are small and not significantly different from the internal variability. The correlations of the model means (thick lines) are larger than for the individual simulations as there is less influence of internal variability than in the individual simulations. As a result, the model means depart from the control run 5%–95% interval earlier, between 1930 and 1960. The multimodel ensemble mean correlation emerges from the internal variability 5%–95% in the 1920s, as there is even more averaging. The correlations of the model means and ensemble mean drop in the 1950–60 period and stabilize from 1980 onward between -0.6 and -0.8. Figure 9 suggests that, in a formal detection and attribution study, the analysis might start in 1950, since the correlations in the period 1950–2005 are detectably different from internal variability while the aerosol and GHG response is not yet perfectly correlated. This implies the use of data before the satellite era, such as ocean reanalyses or reconstructions.

We note that the greenhouse gases are well mixed in the atmosphere, and thus the forced response is driven by the total concentration of GHG in the atmosphere (Meinshausen et al. 2011). In contrast, aerosols are generally short-lived and comprise a variety of aerosol species, which are emitted in different locations and during different time periods as economies around the world develop (Lamarque et al. 2010). The impacts of aerosols on the radiative forcing, particularly the indirect effects, are poorly understood in comparison to the effect of well mixed greenhouse gases. As a result of these factors, the historical pattern of the aerosol forcing may not be scalable to the global aerosol concentration into the future, as the emission magnitudes and locations will likely change. The attribution question may therefore be better answered by simulating the DSL pattern forced by aerosol emissions from certain regions separately and combining these aerosol fingerprints to explain the observed changes.

6. Conclusions

This paper has demonstrated the influence of a range of external forcings on the global mean thermosteric sea level (GMTSL) and on the dynamic sea level change (DSL) in climate models. For this, we used simulations from the CMIP5 archive for the period 1861–2005 driven by five different external forcing combinations: natural only, GHG only, aerosol only, anthropogenic only, and historical.

In GMTSL, the influence of the forcings is clearly distinguishable: while anthropogenic aerosol forcing causes sea level to fall as a result of decreased radiative forcing, increased GHG forcing leads to a sea level rise in the global mean. The natural-only forced experiments show the influence of volcanic forcing on GMTSL, with some models exhibiting a negative bias as a result of absence of volcanic forcing in the preindustrial control run.

The DSL trends are highly variable in time and in space, and again there are clear differences between the five forcing experiments, as shown by long-term trends and EOF analysis. The response of the DSL trends to anthropogenic forcings is significantly different from the response to internal climate variability only, both in spatial pattern and in magnitude. The response of DSL trends to natural-only forcing is smaller and much closer to the internal variability. While the spread in the DSL trend between different realizations from the same model is consistent with the spread in the internal variability (DSL trends derived from the preindustrial control runs), the spread in response to external forcings between the different models is larger, mainly in regions with large DSL trends.

The correlation between the historical DSL time series and the leading EOFs of each of the five historical forcing experiments shows that the pattern associated with GHG already emerges early in the twentieth century, although the initial amplitude of the pattern is small. While the GHG and aerosol-forced responses are highly correlated in GMTSL (~ -0.99), making the two forcings indistinguishable, the correlation is smaller in DSL (-0.76 for the ensemble mean), time dependent, and emerges from the 5%–95% range in internal variability between 1930 and 1960, depending on the model.

Feedback effects between different forcings are examined by comparing the historical-forced response to the anthropogenic + natural forced response (historical comparison) and the anthropogenic-forced response to the GHG + aerosol-forced response (anthropogenic comparison). The differences are small and localized in the historical comparison, while the anthropogenic comparison shows larger differences in more locations, which may be related to both nonlinear feedback effects and unresolved anthropogenic forcings.

The largest forced DSL response is in the Southern Ocean, where the GHG experiments show zonal mean DSL trend peaks at 41°S and a minimum at 69°S. The DSL response to the aerosol experiments shows a positive trend everywhere south of 41°S and a maximum at 58°S. The combination of these two forcings in the anthropogenic experiment results in a minimum around 62°S and a maximum around 41°S. The regional DSL trends are closely related to changes in surface wind stress in response to external forcings.

Both the zonal mean DSL trends and the correlations of GHG and aerosol-forced responses in DSL suggest that there is a chance to separate GHG and aerosol-forced responses in sea level observations, provided that the observations used are of sufficient quality and length. Future work will focus on distinguishing the contributions of the forcings found in the models in observed sea level change patterns.

Acknowledgments. We acknowledge the World Climate Research Programme's Working Group on Coupled Modelling, which is responsible for CMIP, and we thank the climate modeling groups (listed in Table 1 of this paper) for producing and making available their model output. For CMIP, the U.S. Department of Energy's Program for Climate Model Diagnosis and Intercomparison provides coordinating support and led development of software infrastructure in partnership with the Global Organization for Earth System Science Portals. We thank Matt Palmer and James Risbey for commenting on the manuscript. A.S. is funded by a CSIRO Office of the Chief Executive Postdoctoral Fellowship. J.C. and X.Z. are partly funded by the Australian Climate Change Science Program.

REFERENCES

Bellenger, H., E. Guilyardi, J. Leloup, M. Legaigne, and J. Vialard, 2014: ENSO representation in climate models: From CMIP3 to CMIP5. *Climate Dyn.*, **42**, 1999–2018, doi:10.1007/s00382-013-1783-z.

Bilbao, R. A. F., J. M. Gregory, and N. Bouttes, 2015: Analysis of the regional pattern of sea level change due to ocean dynamics and density change for 1993–2099 in observations and CMIP5 AOGCM's. *Climate Dyn.*, doi:10.1007/s00382-015-2499-z, in press.

Bindoff, N., and Coauthors, 2013: Detection and attribution of climate change: From global to regional. *Climate Change 2013: The Physical Science Basis*, T. F. Stocker et al., Eds., Cambridge University Press, 867–952. [Available online at http://www.climatechange2013.org/images/report/WG1AR5_Chapter10_FINAL.pdf.]

Böning, C. W., A. Dispert, M. Visbeck, S. R. Rintoul, and F. U. Schwarzkopf, 2008: The response of the Antarctic Circumpolar Current to recent climate change. *Nat. Geosci.*, **1**, 864–869, doi:10.1038/ngeo362.

Bordbar, M. H., T. Martin, M. Latif, and W. Park, 2015: Effects of long-term variability on projections of twenty-first century dynamic sea level. *Nat. Climate Change*, **5**, 343–347, doi:10.1038/nclimate2569.

Bouttes, N., and J. M. Gregory, 2014: Attribution of the spatial pattern of CO_2-forced sea level change to ocean surface flux changes. *Environ. Res. Lett.*, **9**, 034004, doi:10.1088/1748-9326/9/3/034004.

——, ——, T. Kuhlbrodt, and T. Suzuki, 2012: The effect of windstress change on future sea level change in the Southern Ocean. *Geophys. Res. Lett.*, **39**, L23602, doi:10.1029/2012GL054207.

——, ——, ——, and R. S. Smith, 2014: The drivers of projected North Atlantic sea level change. *Climate Dyn.*, **43**, 1531–1544, doi:10.1007/s00382-013-1973-8.

Carson, M., A. Köhl, and D. Stammer, 2015: The impact of regional multidecadal and century-scale internal climate variability on sea level trends in CMIP5 models. *J. Climate*, **28**, 853–861, doi:10.1175/JCLI-D-14-00359.1.

Christensen, J., and Coauthors, 2013: Climate phenomena and their relevance for future regional climate change. *Climate Change 2013: The Physical Science Basis*, T. F. Stocker et al., Eds., Cambridge University Press, 14SM-1–14SM-62. [Available

online at http://www.ipcc.ch/pdf/assessment-report/ar5/wg1/supplementary/WG1AR5_Ch14SM_FINAL.pdf.]

Church, J., N. J. White, and J. M. Arblaster, 2005: Significant decadal-scale impact of volcanic eruptions on sea level and ocean heat content. *Nature*, **438**, 74–77, doi:10.1038/nature04237.

——, and Coauthors, 2013: Sea level change. *Climate Change 2013: The Physical Science Basis*, T. F. Stocker et al., Eds., Cambridge University Press, 1137–1141. [Available online at http://www.ipcc.ch/pdf/assessment-report/ar5/wg1/WG1AR5_Chapter13_FINAL.pdf.]

Collins, M., and Coauthors, 2013: Long-term climate change: Projections, commitments and irreversibility. *Climate Change 2013: The Physical Science Basis*, T. F. Stocker et al., Eds., Cambridge University Press, 1029–1136. [Available online at http://www.ipcc.ch/pdf/assessment-report/ar5/wg1/WG1AR5_Chapter12_FINAL.pdf.]

Domingues, C. M., J. A. Church, N. J. White, P. J. Gleckler, S. E. Wijffels, P. M. Barker, and J. R. Dunn, 2008: Improved estimates of upper-ocean warming and multi-decadal sea-level rise. *Nature*, **453**, 1090–1094, doi:10.1038/nature07080.

Flato, G., and Coauthors, 2013: Evaluation of climate models. *Climate Change 2013: The Physical Science Basis*, T. F. Stocker et al., Eds., Cambridge University Press, 741–866. [Available online at http://www.ipcc.ch/pdf/assessment-report/ar5/wg1/WG1AR5_Chapter09_FINAL.pdf.]

Frankcombe, L., P. Spence, A. M. Hogg, M. H. England, and S. M. Griffies, 2013: Sea level changes forced by Southern Ocean winds. *Geophys. Res. Lett.*, **40**, 5710–5715, doi:10.1002/2013GL058104.

Gleckler, P. J., K. AchutaRao, J. M. Gregory, B. D. Santer, K. E. Taylor, and T. M. L. Wigley, 2006: Krakatoa lives: The effect of volcanic eruptions on ocean heat content and thermal expansion. *Geophys. Res. Lett.*, **33**, L17702, doi:10.1029/2006GL026771.

Gregory, J. M., 2010: Long-term effect of volcanic forcing on ocean heat content. *Geophys. Res. Lett.*, **37**, L22701, doi:10.1029/2010GL045507.

——, J. A. Lowe, and S. F. B. Teit, 2006: Simulated global-mean sea level changes over the last half-millenium. *J. Climate*, **19**, 4576–4591, doi:10.1175/JCLI3881.1.

——, and Coauthors, 2013: Climate models without preindustrial volcanic forcing underestimate historical ocean thermal expansion. *Geophys. Res. Lett.*, **40**, 1600–1604, doi:10.1002/grl.50339.

Grose, M. R., and Coauthors, 2014: Assessment of the CMIP5 global climate model simulations of the western tropical Pacific climate system and comparison to CMIP3. *Int. J. Climatol.*, **34**, 3382–3399, doi:10.1002/joc.3916.

Hu, A., and C. Deser, 2013: Uncertainty in future regional sea level rise due to internal climate variability. *Geophys. Res. Lett.*, **40**, 2768–2772, doi:10.1002/grl.50531.

Ishii, M., and M. Kimoto, 2009: Reevaluation of historical ocean heat content variations with time-varying XBT and MBT depth bias corrections. *J. Oceanogr.*, **65**, 287–299, doi:10.1007/s10872-009-0027-7.

Knutti, R., D. Masson, and A. Gettelman, 2013: Climate model genealogy: Generation CMIP5 and how we got there. *Geophys. Res. Lett.*, **40**, 1194–1199, doi:10.1002/grl.50256.

Lamarque, J.-F., and Coauthors, 2010: Historical (1850–2000) gridded anthropogenic and biomass burning emissions of reactive gases and aerosols: Methodology and application. *Atmos. Chem. Phys.*, **10**, 7017–7039, doi:10.5194/acp-10-7017-2010.

Levitus, S., and Coauthors, 2012: World ocean heat content and thermosteric sea level change (0–2000 m), 1955–2010. *Geophys. Res. Lett.*, **39**, L10603, doi:10.1029/2012GL051106.

Lewis, S. C., and D. J. Karoly, 2014: Assessment of forced responses of the Australian Community Climate and Earth System Simulator (ACCESS) 1.3 in CMIP5 historical detection and attribution experiments. *Aust. Meteor. Oceanogr. J.*, **64**, 87–101.

Lu, J., A. Hu, and Z. Zeng, 2014: On the possible interaction between internal climate variability and forced climate change. *Geophys. Res. Lett.*, **41**, 2962–2970, doi:10.1002/2014GL059908.

Lyu, K., X. Zhang, J. A. Church, A. B. A. Slangen, and J. Hu, 2014: Time of emergence for regional sea-level change. *Nat. Climate Change*, **4**, 1006–1010, doi:10.1038/nclimate2397.

Mann, M. E., M. A. Cane, S. E. Zebiak, and A. Clement, 2005: Volcanic and solar forcing of the tropical Pacific over the past 1000 years. *J. Climate*, **18**, 447–456, doi:10.1175/JCLI-3276.1.

Mantua, N. J., S. Hare, Y. Zhang, J. Wallace, and R. Francis, 1997: A Pacific interdecadal climate oscillation with impacts on salmon production. *Bull. Amer. Meteor. Soc.*, **78**, 1069–1079, doi:10.1175/1520-0477(1997)078<1069:APICOW>2.0.CO;2.

Marcos, M., and A. Amores, 2014: Quantifying anthropogenic and natural contributions to thermosteric sea level rise. *Geophys. Res. Lett.*, **41**, 2502–2507, doi:10.1002/2014GL059766.

Meehl, G. A., C. Covey, T. Delworth, M. Latif, B. McAvaney, J. F. B. Mitchell, R. J. Stouffer, and K. E. Taylor, 2007: The WCRP CMIP3 multimodel dataset: A new era in climate change research. *Bull. Amer. Meteor. Soc.*, **88**, 1383–1394, doi:10.1175/BAMS-88-9-1383.

Meinshausen, M., and Coauthors, 2011: The RCP greenhouse gas concentrations and their extensions from 1765 to 2300. *Climatic Change*, **109**, 213–241, doi:10.1007/s10584-011-0156-z.

Monselesan, D. P., T. J. O'Kane, J. S. Risbey, and J. A. Church, 2015: Internal climate memory in observations and models. *Geophys. Res. Lett.*, **42**, 1232–1242, doi:10.1002/2014GL062765.

Moss, R. H., and Coauthors, 2010: The next generation of scenarios for climate change research and assessment. *Nature*, **463**, 747–756, doi:10.1038/nature08823.

Myhre, G., and Coauthors, 2013: Anthropogenic and natural radiative forcing. *Climate Change 2013: The Physical Science Basis*, T. F. Stocker et al., Eds., Cambridge University Press, 659–740. [Available online at https://www.ipcc.ch/pdf/assessment-report/ar5/wg1/WG1AR5_Chapter08_FINAL.pdf.]

Nidheesh, A., M. Lengaigne, J. Vialard, A. Unnikrishnan, and H. Dayan, 2013: Decadal and long-term sea level variability in the tropical Indo-Pacific Ocean. *Climate Dyn.*, **41**, 381–402, doi:10.1007/s00382-012-1463-4.

O'Kane, T. J., R. J. Matear, M. A. Chamberlain, J. S. Risbey, B. M. Sloyan, and I. Horenko, 2013: Decadal variability in an OGCM Southern Ocean: Intrinsic modes, forced modes and metastable states. *Ocean Modell.*, **69**, 1–21, doi:10.1016/j.ocemod.2013.04.009.

Pardaens, A. K., J. A. Lowe, S. Brown, R. J. Nicholls, and D. de Gusmao, 2011: Sea-level rise and impacts projections under a future scenario with large greenhouse gas emission reductions. *Geophys. Res. Lett.*, **38**, L12604, doi:10.1029/2011GL047678.

Piecuch, C. G., and R. M. Ponte, 2011: Mechanisms of interannual steric sea level variability. *Geophys. Res. Lett.*, **38**, L15605, doi:10.1029/2011GL048440.

——, and ——, 2012: Buoyancy-driven interannual sea level changes in the southeast tropical Pacific. *Geophys. Res. Lett.*, **39**, L05607, doi:10.1029/2012GL051130.

Power, S., T. Casey, C. Folland, A. Colman, and V. Mehta, 1999: Inter-decadal modulation of the impact of ENSO on Australia. *Climate Dyn.*, **15**, 319–324, doi:10.1007/s003820050284.

Purkey, S. G., and G. C. Johnson, 2010: Warming of global abyssal and deep Southern Ocean waters between the 1990s and 2000s: Contributions to global heat and sea level rise budgets. *J. Climate*, **23**, 6336–6351, doi:10.1175/2010JCLI3682.1.

Rhein, M., and Coauthors, 2013: Observations: Ocean. *Climate Change 2013: The Physical Science Basis*, T. F. Stocker et al., Eds., Cambridge University Press, 255–315. [Available online at https://www.ipcc.ch/pdf/assessment-report/ar5/wg1/WG1AR5_Chapter03_FINAL.pdf.]

Robock, A., 2000: Volcanic eruptions and climate. *Rev. Geophys.*, **38**, 191–219, doi:10.1029/1998RG000054.

Sen Gupta, A., N. C. Jourdain, J. N. Brown, and D. Monselesan, 2013: Climate drift in CMIP5 models. *J. Climate*, **26**, 8597–8615, doi:10.1175/JCLI-D-12-00521.1.

Slangen, A. B. A., C. A. Katsman, R. S. W. van de Wal, L. L. A. Vermeersen, and R. E. M. Riva, 2012: Towards regional projections of twenty-first century sea-level change based on IPCC SRES scenarios. *Climate Dyn.*, **38**, 1191–1209, doi:10.1007/s00382-011-1057-6.

——, M. Carson, C. Katsman, R. van de Wal, A. Koehl, L. Vermeersen, and D. Stammer, 2014a: Projecting twenty-first century regional sea-level changes. *Climatic Change*, **124**, 317–332, doi:10.1007/s10584-014-1080-9.

——, J. A. Church, X. Zhang, and D. Monselesan, 2014b: Detection and attribution of global mean thermosteric sea-level change. *Geophys. Res. Lett.*, **41**, 5951–5959, doi:10.1002/2014GL061356.

Stenchikov, V., T. L. Delworth, V. Ramaswamy, R. J. Stouffer, A. Wittenberg, and F. Zeng, 2009: Volcanic signals in oceans. *J. Geophys. Res.*, **114**, D16104, doi:10.1029/2008JD011673.

Swingedouw, D., P. Ortega, J. Mignot, E. Guilyardi, V. Masson-Delmotte, P. G. Butler, M. Khodri, and R. Séférian, 2015: Bidecadal North Atlantic ocean circulation variability controlled by timing of volcanic eruptions. *Nat. Commun.*, **6**, 6545, doi:10.1038/ncomms7545.

Taylor, K. E., R. J. Stouffer, and G. A. Meehl, 2009: A summary of the CMIP5 experiment design. PCMDI Tech. Rep., 33 pp. [Available online at http://cmip-pcmdi.llnl.gov/cmip5/docs/Taylor_CMIP5_design.pdf.]

——, ——, and ——, 2012: An overview of CMIP5 and the experiment design. *Bull. Amer. Meteor. Soc.*, **93**, 485–498, doi:10.1175/BAMS-D-11-00094.1.

Timmermann, A., S. McGregor, and F.-F. Jin, 2010: Wind effects on past and future regional sea level trends in the southern Indo-Pacific. *J. Climate*, **23**, 4429–4437, doi:10.1175/2010JCLI3519.1.

Yin, J., 2012: Century to multi-century sea level rise projections from CMIP5 models. *Geophys. Res. Lett.*, **39**, doi:10.1029/2012GL052947.

——, M. E. Schlesinger, and R. J. Stouffer, 2009: Model projections of rapid sea-level rise on the northeast coast of the United States. *Nat. Geosci.*, **2**, 262–266, doi:10.1038/ngeo462.

——, S. M. Griffies, and R. J. Stouffer, 2010: Spatial variability of sea-level rise in twenty-first century projections. *J. Climate*, **23**, 4585–4607, doi:10.1175/2010JCLI3533.1.